Exploring the control landscape for nonlinear quantum dynamics

Julia Yan, David Hocker, Ruixing Long, Tak-San Ho, and Herschel Rabitz*
Department of Chemistry, Princeton University, Princeton, New Jersey 08544, USA
(Received 27 February 2014; published 10 June 2014)

Manipulation of a quantum system can be viewed in the framework of a *control landscape* defined as the physical objective as a functional of the control. Control landscape analyses have thus far considered linear quantum dynamics. This paper extends the analysis of control landscape topology to nonlinear quantum dynamics with the objective of steering a finite-level quantum system from an initial state to a final target state. The analysis rests on the assumptions that (i) the final state is reachable from the initial state, (ii) the differential mapping from the control to the state is surjective, and (iii) the control resources are unconstrained. Under these assumptions, landscape critical points (i.e., where the slope vanishes) for nonlinear quantum dynamics only appear as the global maximum and minimum; thus, the landscape is free of *traps*. Moreover, the landscape Hessian (i.e., the second derivative with respect to the control) at the global maximum has finite rank, indicating the presence of a large *level set* of optimal controls that preserve the value of the maximum. Extensive numerical simulations on finite-level models of the Gross-Pitaevskii equation confirm the trap-free nature of the landscape as well as the Hessian rank analysis, using either an applied electric field or a tunable condensate two-body interaction strength as the control. In addition, the control mechanisms arising in the numerical simulations are qualitatively assessed. These results are a generalization of previous findings for the linear Schrödinger equation, and show promise for successful control in a wide range of nonlinear quantum dynamics applications.

DOI: 10.1103/PhysRevA.89.063408 PACS number(s): 32.80.Qk, 67.85.Hj, 02.30.Yy, 05.45.−a

I. INTRODUCTION

The nonlinear Schrödinger equation (NLS) has generated much interest for its significance in modeling quantum many-body problems, where the nonlinearity enters from taking a mean-field approximation of particle-particle interactions. In addition, the NLS arises in other domains including classical nonlinear optics, where the nonlinear term is a result of photon-photon interactions induced by the optical medium [1]. Most notably, the NLS appears in modeling the dynamics of Bose-Einstein condensates (BECs) [2], where the focus is on the Gross-Pitaevskii equation (GPE), forming a special case of the NLS with a cubic nonlinearity that models two-particle collisions in the condensate. The study of BECs is of fundamental interest [3–8], as well as for applications [9–16]. Prior control work with the GPE has mainly focused on using a parametrized trapping potential as a control; recent numerical studies have demonstrated transport [17,18] and wave-function splitting [19] through the manipulation of magnetic trapping potentials, and a superposition of two states has been achieved using frequency detuning between laser beams to form an optical lattice [20]. A novel control parameter is the strength of the nonlinear term in the Hamiltonian, where magnetic fields [21–23] or optical methods [24] have been proposed to tune the two-body interaction strength through Feshbach resonances.

This work aims to explore the control of nonlinear quantum dynamics through *landscape analysis*, where the landscape is the physical objective $J[c(t)]$ as a functional of the control $c(t)$. Extensive recent studies have examined the landscape topology for the control of linear quantum dynamical phenomena [25,26], where the control goal can be written as the following maximization problem:

$$\max_{c(t)} J[c(t)]. \tag{1}$$

The controls may be either an applied time-dependent field [26] or manipulation of the internal structure of the Hamiltonian through system engineering [27]. The maximization goal in Eq. (1) also applies to optimal control objectives with NLS dynamics.

This optimization can be viewed as a search over the control landscape $J[c(t)]$. Analysis of the landscape topology is important in determining the feasibility of seeking control over nonlinear quantum dynamics phenomena. To this end, a first-order analysis focuses on the location of the landscape critical points, i.e., where $\delta J/\delta c(t) = 0$ for all $t \in [0,T]$, with T being the final time at which the control objective $J[c(t)]$ is evaluated; a second-order analysis using the Hessian $\delta^2 J/\delta c(t)\delta c(t')$ allows for classification of the critical points, which could correspond to global maxima, global minima, suboptimal extrema, or saddles [25,26]. This work considers the state-to-state control objective $J[c(t)] \equiv P_{i\to f}(T)$, where $P_{i\to f}(T)$ is the transition probability between initial state $|\phi_i\rangle$ and target state $|\phi_f\rangle$.

Landscape analysis has thus far been restricted to the linear Schrödinger equation in an N-state basis. Three important assumptions underlie the prior analysis [25,26,28,29]: (i) the final target state $|\phi_f\rangle$ can be reached from the initial state $|\phi_i\rangle$, (ii) the mapping of the control to the system state at time T is surjective, and (iii) the control is unconstrained. Although any of the assumptions could be violated, the satisfaction of (i) and (ii) appear to be easy for reasonable physical systems. A primary concern is assumption (iii), as control resources are always limited in the laboratory. However, the practical issue is the availability of adequate resources to meet the objective in Eq. (1) to a desired degree. Upon satisfaction of these assumptions, analysis of the linear Schrödinger equation

*Corresponding author: hrabitz@princeton.edu

shows that the landscape is trap free [25], with no suboptimal extrema which could halt a gradient-based climbing algorithm when searching for the top of the landscape. Furthermore, the Hessian is shown to have an infinite-dimensional null space at the top and bottom of the landscape. In particular, for the objective $J[c(t)] = P_{i\to f}(T)$, the Hessian has rank of at most $2N-2$ at the top and at most 2 at the bottom [26]. The finite rank of the Hessian results in *level sets* of controls that preserve the value of $P_{i\to f}(T)$, and the level sets may be explored by moving through the Hessian null space [27]. In addition, the presence of a family of optimal control solutions indicates an inherent degree of robustness to noise [26–28].

The attractive landscape behavior outlined above for linear quantum dynamics provides a basis to explain the evident relative ease of finding effective controls. This paper aims to generalize the landscape analysis to treat nonlinear quantum dynamics based on the same three assumptions utilized in linear quantum dynamics for the basic case of $J[c(t)] = P_{i\to f}(T)$. We will show that under these assumptions, the same favorable landscape topological conclusions arise for control of the NLS. To support the conclusions, optimal control simulations are performed with the GPE considering either an electric field or the nonlinear coupling coefficient as the time-dependent control. The simulations are performed by discretizing the GPE in a finite basis set of size N. The remaining sections of the paper are organized as follows. Section II presents the N-level NLS and GPE models, while Sec. III provides details for the formulation of the control problem for nonlinear quantum dynamics. Section IV presents a Dyson-type expansion for the NLS to provide a basis to qualitatively assess the control mechanism as well as the physical origin of the structure in the Hessian eigenvectors in the simulations. The latter development of the means to relate the features of NLS simulations to the underlying NLS physical model follows extensive continuing interest in control mechanism assessment for dynamics described by the linear Schrödinger equation. Section V summarizes the gradient-based methods to climb the landscape and the Hessian-based procedure to traverse the control landscape top or bottom level sets [30,31]. Control simulations are presented in Sec. VI, and concluding remarks are given in Sec. VII.

II. PHYSICAL SYSTEM DESCRIPTION

This section outlines the nature of the physical systems for landscape analysis of Sec. III. The NLS of arbitrary nonlinearity, as well as the special case of the GPE, will be considered. As with prior landscape analyses of the linear Schrödinger equation [25,26], the NLS and the GPE will be represented in a finite basis set of size N.

A. N-level nonlinear Schrödinger equation

The general NLS in the presence of a time-dependent control $c(t)$ is written in the following form (taking $\hbar = 1$) [32,33]:

$$i\frac{\partial}{\partial t}\psi(r,t) = (\hat{H}^{(0)} + \hat{H}^{(1)}[\psi(r,t),\psi^*(r,t);\ c(t)])\psi(r,t), \quad (2)$$

where $\psi(r,t)$ specifies the state of the system (i.e., the so-called *order parameter* in the context of BECs) at time t and position r, and $\hat{H}^{(0)}$ is the control-free Hamiltonian which is independent of $\psi(r,t)$. Here, the term $\hat{H}^{(1)}[\psi(r,t),\psi^*(r,t);\ c(t)]\psi(r,t)$ depends on the control $c(t)$ and includes the nonlinearity in $\psi(r,t)$. We note that $\hat{H}^{(1)}[\psi(r,t),\psi^*(r,t);\ c(t)]\psi(r,t)$ may also include terms that are linear in $\psi(r,t)$ as occurs with the linear Schrödinger equation. For the Hamiltonian $\hat{H} = \hat{H}^{(0)} + \hat{H}^{(1)}[\psi(r,t),\psi^*(r,t);\ c(t)]$, physical relevance requires that the expectation value $\langle\hat{H}\rangle$ be real, such that the norm of $\psi(r,t)$ is conserved (taken as 1 here). This requirement implies that $\psi(r,t)$ and $\psi^*(r,t)$ must enter symmetrically into $\hat{H}^{(1)}[\psi(r,t),\psi^*(r,t);\ c(t)]$. In addition, for simplicity of the subsequent analysis, the control $c(t)$ is taken to be a scalar without spatial dependence, although the extension can be easily considered.

The special reduced form of Eq. (2) for application in BECs is the GPE

$$i\frac{\partial}{\partial t}\psi(r,t) = (\hat{H}^{(0)} + V(r,t) + g(t)|\psi(r,t)|^2)\psi(r,t), \quad (3)$$

where $V(r,t)$ is an applied potential and $g = 4\pi a_s/m$ is the two-body coupling coefficient (possibly time dependent) related to the scattering length a_s, and m is the mass of the condensate atoms [2]. In this work, we consider the potential in Eq. (3) to have the form $V(r,t) = -\hat{\mu}(r)\varepsilon(t)$, where $\varepsilon(t)$ is a time-dependent electric field and $\hat{\mu}(r)$ is the dipole moment. Other forms of the potential could be treated as well. Thus, in Eq. (3) the control $c(t)$ may be either $\varepsilon(t)$ or $g(t)$.

In order to perform the landscape analysis and numerically simulate control of NLS dynamics, we recast Eq. (2) in a finite basis $\{\phi_n(r) = \langle r \mid \phi_n\rangle\}$ by expanding the wave function $\psi(r,t)$ in terms of the coefficients $\psi_n(t)$:

$$\psi(r,t) = \sum_{n=1}^{N}\psi_n(t)\phi_n(r), \quad (4)$$

where N is sufficiently large to capture the relevant dynamics of $\psi(r,t)$, and the basis set $\{\phi_n(r)\}$ is orthonormal such that $\int dr\,\phi_m^*(r)\phi_n(r) = \delta_{mn}$. Substituting Eq. (4) for $\psi(r,t)$ in Eq. (2), multiplying by $\phi_m^*(r)$ on the left, and integrating, gives the following equation of motion for $\psi_m(t)$:

$$i\frac{d}{dt}\psi_m(t) = \sum_{n=1}^{N}H_{mn}^{(0)}\psi_n(t) + \sum_{n=1}^{N}\psi_n(t)H_{mn}^{(1)}[\psi(t),\psi^*(t);\ c(t)], \quad (5)$$

where the $N\times N$ matrices $H^{(0)}$ and $H^{(1)}[\psi(t),\psi^*(t);\ c(t)]$ have the following matrix elements:

$$H_{mn}^{(0)} = \int dr\,\phi_m^*(r)\hat{H}^{(0)}\phi_n(r), \quad (6a)$$

$$H_{mn}^{(1)}[\psi(t),\psi^*(t);\ c(t)] = \int dr\,\phi_m^*(r)\hat{H}^{(1)} \times [\psi(r,t),\psi^*(r,t);\ c(t)]\phi_n(r). \quad (6b)$$

To facilitate the analysis of Eq. (5), the system state $|\psi(t)\rangle$ in the finite basis is written as the column vector

$$|\psi(t)\rangle = [\psi_1(t), \quad \psi_2(t)\ldots\psi_N(t)]^{\mathrm{T}}, \quad (7a)$$

where T denotes the matrix transpose operation. Similarly, $\langle\psi(t)|$ denotes the row vector

$$\langle\psi(t)| = [\psi_1^*(t), \quad \psi_2^*(t)\ldots\psi_N^*(t)]. \tag{7b}$$

Equation (5) may now be written as a set of N coupled ordinary differential equations

$$i\frac{d}{dt}|\psi(t)\rangle = (H^{(0)} + H^{(1)}[\psi(t),\psi^*(t);\ c(t)])|\psi(t)\rangle, \tag{8}$$

where $\psi(t)$ and $\psi^*(t)$ in $H^{(1)}[\psi(t),\psi^*(t);\ c(t)]$ have the corresponding vector components in Eqs. (7a) and (7b).

B. *N*-level Gross-Pitaevskii equation

For the special case of the GPE, $\hat{H}^{(1)}[\psi(r,t),\psi^*(r,t);\ \varepsilon(t),g(t)] = -\hat{\mu}(r)\varepsilon(t) + g(t)|\psi(r,t)|^2$ with two possible controls $c(t) \to \varepsilon(t),g(t)$. In this case, Eq. (8) takes the specific form

$$i\frac{d}{dt}|\psi(t)\rangle = (H^{(0)} - \mu\varepsilon(t) + g(t)M[\psi(t),\psi^*(t)])|\psi(t)\rangle. \tag{9}$$

The matrix elements of $H^{(1)}[\psi(t),\psi^*(t);\ \varepsilon(t),g(t)]$ are

$$H_{mn}^{(1)}[\psi(t),\psi^*(t);\ \varepsilon(t),g(t)] = -\mu_{mn}\varepsilon(t) + g(t)M_{mn}[\psi(t),\psi^*(t)], \tag{10}$$

where μ_{mn} is an element of the transition dipole moment $\mu_{mn} = \int dr\phi_m^*(r)\hat{\mu}(r)\phi_n(r)$, and $M[\psi(t),\psi^*(t)]$ is an $N \times N$ matrix with entries

$$M_{mn}[\psi(t),\psi^*(t)] = \sum_{k=1}^{N}\sum_{l=1}^{N}\psi_k(t)\psi_l^*(t) \times \int dr\ \phi_m^*(r)\phi_l^*(r)\phi_k(r)\phi_n(r). \tag{11}$$

Prior work on approximating the GPE with a finite-basis-set expansion includes use of harmonic oscillator functions [34], Wannier functions [35], and Chebyshev polynomials [36], as well as the eigenstates of the linear portion of the Hamiltonian with a trapping potential [37–39]. The controllability of these finite-level nonlinear quantum systems has yet to be established, and this issue is complex even for linear quantum dynamics [26,40–42]. In this regard, we assume satisfaction of assumption (i) that the target state $|\phi_f\rangle$ can be reached from the initial state $|\phi_i\rangle$. In the analysis of the GPE dynamics that follows, we assume that the basis $\{\phi_n(r)\}$ are eigenstates of $H^{(0)}$ with eigenvalues $\{E_n\}$, and the initial and final states $|\phi_i\rangle$ and $|\phi_f\rangle$ are drawn from these eigenstates.

III. CONTROL LANDSCAPE ANALYSIS

With the quantum system described by Eq. (8), the objective is to find an optimal control that can guide the dynamics from initial state $|\phi_i\rangle$ at time $t = 0$ to a desired final state $|\phi_f\rangle$ at time $t = T$. For this situation,

$$P_{i\to f}(T) = |\langle\phi_f \mid \psi(T)\rangle|^2, \tag{12}$$

and $|\psi(0)\rangle = |\phi_i\rangle$. The following subsections will analyze the landscape in Eq. (12) by first identifying the critical points and then assessing their nature by consideration of the associated Hessian spectrum.

A. Identification of critical points

The critical-point analysis calls for identifying the conditions when $\delta P_{i\to f}(T)/\delta c(t) = 0$, $t \in [0,T]$. These critical points are denoted as *dynamical*, and generally include global maxima, global minima, suboptimal extrema, and saddles. The gradient of $P_{i\to f}(T) = |\langle\phi_f \mid \psi(T)\rangle|^2$ with respect to $c(t)$ is given by

$$\frac{\delta P_{i\to f}}{\delta c(t)} = \left\langle\phi_f\left|\frac{\delta\psi(T)}{\delta c(t)}\right\rangle\langle\psi(T)\mid\phi_f\rangle + \langle\phi_f\mid\psi(T)\rangle\left\langle\frac{\delta\psi(T)}{\delta c(t)}\right|\phi_f\right\rangle = 2\,\mathrm{Re}\left[\left\langle\phi_f\left|\frac{\delta\psi(T)}{\delta c(t)}\right\rangle\langle\psi(T)|\phi_f\rangle\right]. \tag{13}$$

In the analysis, $c(t)$ is either $\varepsilon(t)$ or $g(t)$ in Eq. (8); the more general case of both controls operating simultaneously can be readily treated. We also adopt all three assumptions (i), (ii), and (iii) in Sec. I, which are the same premises employed in a like analysis with the linear Schrödinger equation [25,26,29]. The critical-point condition can be rewritten using the chain rule, i.e. [29],

$$\frac{\delta P_{i\to f}}{\delta c(t)} = \frac{\partial P_{i\to f}}{\partial\psi(T)}\frac{\delta\psi(T)}{\delta c(t)} = 0, \tag{14}$$

where it is understood that $\partial P_{i\to f}/\partial\psi(T)$ is a vector of length $2N$ with elements corresponding to differentiation with respect to the real and imaginary parts of $|\psi(T)\rangle$. Critical points [i.e., $\delta P_{i\to f}/\delta c(t) = 0$] satisfying $\partial P_{i\to f}/\partial\psi(T) = 0$ are referred to as *kinematic*. Considering the validity of the assumption (ii) that surjectivity of the mapping $\delta c(t) \to |\delta\psi(T)\rangle$ is satisfied [i.e., for an arbitrary differential change $|\delta\psi(T)\rangle$ in the final state, there is a corresponding variation $\delta c(t)$ in the control such that $\delta\psi(T)/\delta c(t)$ is full rank], it follows that $\partial P_{i\to f}/\partial\psi(T) = 0$. Thus, $c(t)$ is a critical point of $P_{i\to f}(T)$ if and only if $\psi(T)$ corresponds to a critical point of $P_{i\to f}(T) = |\langle\psi_f \mid \psi(T)\rangle|^2$, and then all critical points are both dynamical and kinematic. The necessary kinematic critical-point analysis of $\partial P_{i\to f}/\partial\psi(T) = 0$ can be performed without further consideration of the control $c(t)$, expressed as

$$\max_{\psi(T)} P_{i\to f}(T) \quad \text{s.t. } \langle\psi(T)\mid\psi(T)\rangle = 1. \tag{15}$$

This constrained optimization problem can be recast with the Lagrange multiplier λ as

$$\max_{\psi(T),\lambda}\mathcal{L}(\psi,\lambda), \tag{16}$$

where

$$\mathcal{L}(\psi,\lambda) = \langle\psi(T)|\phi_f\rangle\langle\phi_f|\psi(T)\rangle + \lambda[1 - \langle\psi(T)|\psi(T)\rangle], \tag{17}$$

with the first-order optimality conditions

$$\frac{\partial\mathcal{L}}{\partial\psi(T)} = \langle\psi(T)|\phi_f\rangle\langle\phi_f| - \lambda\langle\psi(T)| = 0, \tag{18a}$$

$$\frac{\partial\mathcal{L}}{\partial\lambda} = 1 - \langle\psi(T)\mid\psi(T)\rangle = 0. \tag{18b}$$

Projecting Eq. (18a) onto $|\psi(T)\rangle$ and using the normalization condition in Eq. (18b), we have

$$\lambda = \langle\psi(T)\,|\,\phi_f\rangle\langle\phi_f\,|\,\psi(T)\rangle. \tag{19}$$

Substituting Eq. (19) for λ into Eq. (18a), the first-order optimality condition becomes

$$\frac{\partial\mathcal{L}}{\partial\psi(T)} = \langle\psi(T)|\psi_f\rangle(\langle\psi_f| - \langle\psi_f|\psi(T)\rangle\langle\psi(T)|) = 0, \tag{20}$$

which is satisfied if and only if one of the following two relations hold:

(1) $\langle\psi(T)\,|\,\psi_f\rangle = 0$, or

(2) $\langle\psi_f| = \langle\psi_f\,|\,\psi(T)\rangle\langle\psi(T)| \quad\Rightarrow\quad 1 = \langle\psi_f\,|\,\psi(T)\rangle\langle\psi(T)\,|\,\psi_f\rangle$.

The first relation corresponds to $P_{i\to f}(T) = 0$, or the bottom of the landscape; the second relation corresponds to $P_{i\to f}(T) = 1$, or the top of the landscape. Thus, upon satisfaction of assumptions (i), (ii), and (iii) in Sec. I, the only critical points are at the top and bottom of the landscape, and the landscape is trap free. Note that the trap-free result holds for any pure states $|\phi_i\rangle$ and $|\phi_f\rangle$ drawn from the eigenvectors $\{|\phi_n\rangle\}$, as well as for superpositions of these states.

B. Hessian analysis

We seek to assess the nature of the critical points at the bottom and top of the landscape. Of particular interest is whether the Hessian at the top (bottom) is negative (positive) definite or semidefinite. The Hessian can be easily expressed by differentiating Eq. (13):

$$\frac{\delta^2 P_{i\to f}}{\delta c(t)\delta c(t')} = 2\,\mathrm{Re}\left[\left\langle\frac{\delta\psi(T)}{\delta c(t')}\middle|\phi_f\right\rangle\left\langle\phi_f\middle|\frac{\delta\psi(T)}{\delta c(t)}\right\rangle + \langle\psi(T)\,|\,\phi_f\rangle\left\langle\phi_f\middle|\frac{\delta^2\psi(T)}{\delta c(t)\delta c(t')}\right\rangle\right]. \tag{21}$$

Equation (21) applies anywhere on the landscape, and in the following analysis we focus on the bottom and top.

1. Hessian at the landscape bottom

Although being at the bottom of the landscape is not generally desirable, the Hessian character there is important since many initial controls will produce a yield in that vicinity. At the bottom of the landscape, $\langle\phi_f\,|\,\psi(T)\rangle = 0$. Thus, the second variation drops out of Eq. (21), resulting in the expression

$$\frac{\delta^2 P_{i\to f}}{\delta c(t)\delta c(t')} = 2\,\mathrm{Re}\left[\left\langle\frac{\delta\psi(T)}{\delta c(t')}\middle|\phi_f\right\rangle\left\langle\phi_f\middle|\frac{\delta\psi(T)}{\delta c(t)}\right\rangle\right] \tag{22}$$

$$= x(t)x(t') + y(t)y(t'), \tag{23}$$

where

$$x(t) = \sqrt{2}\,\mathrm{Re}\left[\left\langle\frac{\delta\psi(T)}{\delta c(t)}\middle|\phi_f\right\rangle\right], \tag{24a}$$

$$y(t) = \sqrt{2}\,\mathrm{Im}\left[\left\langle\frac{\delta\psi(T)}{\delta c(t)}\middle|\phi_f\right\rangle\right]. \tag{24b}$$

Equation (23) is the sum of two rank-one matrices, so the rank of the Hessian at the bottom is at most two, and the Hessian has an infinite-dimensional null space. From Eq. (23), it is also easy to see that for any continuous nonzero function $w(t)$, $t\in[0,T]$,

$$\int_0^T dt'\int_0^T dt\,\frac{\delta^2 P_{i\to f}}{\delta c(t)\delta c(t')}w(t)w(t') = \left(\int_0^T dt\,x(t)w(t)\right)^2 + \left(\int_0^T dt\,y(t)w(t)\right)^2 \geqslant 0. \tag{25}$$

Therefore, the Hessian at the bottom is positive semidefinite, and has eigenvalues $\lambda_1,\lambda_2 \geqslant 0$, consistent with being at the global minimum. This result implies that if the control $c(t)$ produces the outcome $P_{i\to f}(T) = 0$, then there are at most two linearly independent variations around $c(t)$ that can lift $P_{i\to f}(T)$ off the bottom.

2. Hessian at the landscape top

Since $\langle\psi(T)\,|\,\psi(T)\rangle = 1$, the following relation holds:

$$\frac{\delta^2}{\delta c(t)\delta c(t')}\langle\psi(T)|\psi(T)\rangle = 2\mathrm{Re}\left[\left\langle\frac{\delta\psi(T)}{\delta c(t')}\middle|\frac{\delta\psi(T)}{\delta c(t)}\right\rangle + \left\langle\psi(T)\middle|\frac{\delta^2\psi(T)}{\delta c(t)\delta c(t')}\right\rangle\right] = 0, \tag{26}$$

from which we conclude

$$\mathrm{Re}\left[\left\langle\psi(T)\middle|\frac{\delta^2\psi(T)}{\delta c(t)\delta c(t')}\right\rangle\right] = -\mathrm{Re}\left[\left\langle\frac{\delta\psi(T)}{\delta c(t')}\middle|\frac{\delta\psi(T)}{\delta c(t)}\right\rangle\right]. \tag{27}$$

Substituting Eq. (27) into Eq. (21), and using the relation $|\psi_f\rangle\langle\psi_f| = |\psi(T)\rangle\langle\psi(T)|$ at the top of the landscape, the Hessian can then be written as

$$\begin{aligned}\frac{\delta^2 P_{i\to f}}{\delta c(t)\delta c(t')} &= 2\mathrm{Re}\left[\left\langle\frac{\delta\psi(T)}{\delta c(t')}\middle|\phi_f\right\rangle\left\langle\phi_f\middle|\frac{\delta\psi(T)}{\delta c(t)}\right\rangle - \left\langle\frac{\delta\psi(T)}{\delta c(t')}\middle|\frac{\delta\psi(T)}{\delta c(t)}\right\rangle\right]\\ &= -2\mathrm{Re}\left[\left\langle\frac{\delta\psi(T)}{\delta c(t')}\middle|\Big(\mathbf{I} - |\phi_f\rangle\langle\phi_f|\Big)\middle|\frac{\delta\psi(T)}{\delta c(t)}\right\rangle\right]\\ &= -\sum_{n\neq f}[u_n(t)u_n(t') + v_n(t)v_n(t')],\end{aligned} \tag{28}$$

where

$$u_n(t) = \sqrt{2}\,\mathrm{Re}\left[\left\langle\frac{\delta\psi(T)}{\delta c(t)}\middle|\phi_n\right\rangle\right], \tag{29a}$$

$$v_n(t) = \sqrt{2}\,\mathrm{Im}\left[\left\langle\frac{\delta\psi(T)}{\delta c(t)}\middle|\phi_n\right\rangle\right]. \tag{29b}$$

Noting that $\{|\phi_n\rangle\}$ is a complete set of N-dimensional vectors, then Eq. (28) is the sum of at most $2N-2$ rank-one matrices. Thus, the rank of the Hessian at the top is at most $2N-2$, and the Hessian has an infinite-dimensional null space. From Eq. (28), it is easy to see that for any continuous nonzero

function $w(t)$, $t \in [0,T]$,

$$\int_0^T dt' \int_0^T dt \frac{\delta^2 P_{i\to f}}{\delta c(t)\delta c(t')} w(t)w(t') = -\sum_{n\neq f}\left(\int_0^T dt u(t)w(t)\right)^2 - \sum_{n\neq f}\left(\int_0^T dt v(t)w(t)\right)^2 \leqslant 0. \tag{30}$$

Thus, the Hessian at the top is negative semidefinite, and has eigenvalues $\lambda_1,\lambda_2,\ldots,\lambda_{2N-2} \leqslant 0$, consistent with being at the global maximum. As a result, if $c(t)$ is a control that produces $P_{i\to f}(T) = 1$, then there are at most $2N-2$ linearly independent variations that around $c(t)$ that can take $P_{i\to f}(T)$ off the top. Furthermore, the finite rank of the Hessian indicates that control solutions at the top of the landscape have an inherent degree of robustness to noise [26–28].

This section has generalized the previous landscape analysis for the linear Schrödinger equation [25,26,28,29] to a like treatment for a general form of the NLS. Importantly, upon satisfaction of the three assumptions in Sec. I, the landscape topology conclusions are the same for linear and nonlinear quantum dynamics. The finite rank of the Hessian at the top and bottom of the landscape implies the existence of level sets preserving the value of the objective while moving through the Hessian null space. Section VI numerically verifies the above analyses and demonstrates level-set explorations for the GPE. Beyond the general analysis here, the impact of violating the assumptions is a challenge to explore. This issue is still under study in the case of the linear Schrödinger equation, and experience there suggests that the prime concern for applications in the laboratory is assumption (iii) on the availability of adequate control resources.

IV. CONTROL MECHANISM ASSESSMENT

The primary focus of this work is on analyzing the control landscape topology of the NLS, including the findings in the simulations of Sec. VI. General practice with control of the linear Schrödinger equation is consideration of the control mechanisms leading to optimization of the objective. For the NLS, equally strong motivation exists for assessing control mechanisms and the physical origins of features appearing in the controls and Hessian eigenvectors. A variety of tools have been developed for determining the control-induced dynamical mechanisms within linear Schrödinger equation dynamics, including a Fourier analysis of the control $c(t)$ compared to the transition frequencies in the Hamiltonian, plots of the evolving populations $P_{i\to j}(T)$, $t \in [0,T]$, $\forall\ j$, and determination of the individual amplitudes in the Dyson expansion for the evolving state. These procedures often utilize the interaction representation, or possibly some other reference as a foundation for assessment. Building on the latter considerations, it is convenient to use the interaction representation with the GPE where $|\psi(t)\rangle = \exp[-iH^{(0)}t]|\eta(t)\rangle$. A full study of GPE control mechanism analysis is beyond the scope of this work, but employing the interaction representation with a Dyson-type expansion will be used to provide mechanistic insights in the numerical calculations in Sec. VI, including contributions from the nonlinear term in the Hamiltonian.

The N-level NLS in the interaction representation may be written as

$$i\frac{d}{dt}|\eta(t)\rangle = H_I^{(1)}|\eta(t)\rangle, \tag{31}$$

where

$$H_I^{(1)} = e^{iH^{(0)}t}\ H^{(1)}[e^{-iH^{(0)}t}\eta(t), e^{iH^{(0)}t}\eta^*(t);\ c(t)]\ e^{-iH^{(0)}t}, \tag{32}$$

and for the particular case of the GPE,

$$H_I^{(1)} = -e^{iH_0t}[\mu\varepsilon(t)]e^{-iH_0t} + g(t)e^{iH_0t}\left(M[e^{-iH^{(0)}t}\eta(t), e^{iH^{(0)}t}\eta^*(t)]\right)e^{-iH_0t}. \tag{33}$$

Equation (31) is just as nonlinear as the original NLS, but factoring out the oscillatory free dynamics through $|\psi(t)\rangle = \exp[-iH^{(0)}t]|\eta(t)\rangle$ permits a convenient qualitative assessment of the likely contributing frequency components in the control and in the important eigenvectors of the Hessian matrices. In forming a Dyson-type expansion of Eq. (31), we assume that the control $|c(t)| < c_0\ \forall\ t$ for some constant c_0, such that $\|H_I^{(1)}\|$ is bounded from above considering that the dynamics here lies in a space of finite dimension N and the matrix elements of μ and $M[\psi(t),\psi^*(t)]$ are finite. Thus, despite $H_I^{(1)}$ depending on $|\eta(t)\rangle$, the Dyson expansion of Eq. (31) will converge. We leave the nonlinear contribution intact in Eq. (33), such that each term of the Dyson expansion still depends on $|\eta(t)\rangle$. However, when assuming that $|\eta(t)\rangle$ is slowly varying in time, the expansion still permits an assessment of the likely important resonant frequency components. The Dyson expansion of Eq. (31) combined with Eq. (12) leads to $P_{i\to f}(T)$ having the form

$$P_{i\to f}(T) = |\ p^{(0)} + p^{(1)} + p^{(2)} + \cdots + p^{(n)} + \cdots|^2, \tag{34}$$

where the first few expansion terms $p^{(n)}$ for $n = 0,1,2$ are, respectively, given by

$$p^{(0)} = \langle\phi_f\,|\,\phi_i\rangle = \delta_{if}, \tag{35a}$$

$$p^{(1)} = -i\int_0^T dt\ \langle\phi_f|H_I^{(1)}[e^{-iH^{(0)}t}\eta(t), e^{iH^{(0)}t}\eta^*(t);\ c(t)]|\phi_i\rangle, \tag{35b}$$

$$p^{(2)} = (-i)^2\sum_m\int_0^T dt\int_0^t dt' \times\langle\phi_f|H_I^{(1)}[e^{-iH^{(0)}t}\eta(t), e^{iH^{(0)}t}\eta^*(t);\ c(t)]|\phi_m\rangle \times\langle\phi_m|H_I^{(1)}[e^{-iH^{(0)}t'}\eta(t'), e^{iH^{(0)}t'}\eta^*(t');\ c(t')]|\phi_i\rangle. \tag{35c}$$

For the GPE, these terms become

$$p^{(0)} = \langle\phi_f\,|\,\phi_i\rangle, \tag{36a}$$

$$p^{(1)} = i\int_0^T dt\ e^{i(E_f-E_i)t}\langle\phi_f|\mu|\phi_i\rangle\varepsilon(t) - i\int_0^T dt\ e^{i(E_f-E_i)t}\langle\phi_f|M[e^{-iH^{(0)}t}\eta(t), \times e^{iH^{(0)}t}\eta^*(t)]|\phi_i\rangle g(t), \tag{36b}$$

$$p^{(2)} = p_a^{(2)} + p_b^{(2)} + p_c^{(2)} + p_d^{(2)}, \tag{36c}$$

where $p_a^{(2)}, p_b^{(2)}, p_c^{(2)}$, and $p_d^{(2)}$ are, respectively, given as

$$p_a^{(2)} = (-i)^2 \sum_m \int_0^T dt \int_0^t dt'\, e^{i(E_f - E_m)t} \langle \phi_f | \mu | \phi_m \rangle \varepsilon(t) \times e^{i(E_m - E_i)t'} \langle \phi_m | \mu | \phi_i \rangle \varepsilon(t'), \tag{37a}$$

$$p_b^{(2)} = -(-i)^2 \sum_m \int_0^T dt \int_0^t dt'\, e^{i(E_f - E_m)t} \langle \phi_f | \mu | \phi_m \rangle \varepsilon(t) \times e^{i(E_m - E_i)t'} \langle \phi_m | M[e^{-iH^{(0)}t'} \eta(t'), e^{iH^{(0)}t'} \eta^*(t')] | \phi_i \rangle g(t'), \tag{37b}$$

$$p_c^{(2)} = -(-i)^2 \sum_m \int_0^T dt \int_0^t dt' e^{i(E_f - E_m)t} \langle \phi_f | M[e^{-iH^{(0)}t} \eta(t), e^{iH^{(0)}t} \eta^*(t)] | \phi_m \rangle g(t) e^{i(E_m - E_i)t'} \langle \phi_m | \mu | \phi_i \rangle \varepsilon(t'), \tag{37c}$$

$$p_d^{(2)} = (-i)^2 \sum_m \int_0^T dt \int_0^t dt'\, e^{i(E_f - E_m)t} \langle \phi_f | M[e^{-iH^{(0)}t} \eta(t), e^{iH^{(0)}t} \eta^*(t)] | \phi_m \rangle g(t) e^{i(E_m - E_i)t'} \langle \phi_m | M[e^{-iH^{(0)}t'} \eta(t'), e^{iH^{(0)}t'} \eta^*(t')] | \phi_i \rangle g(t'), \tag{37d}$$

and the elements of $M[e^{-iH^{(0)}t}\eta(t), e^{iH^{(0)}t}\eta^*(t)]$ are [cf. Eq. (11)]

$$M_{mn}[e^{-iH^{(0)}t}\eta(t), e^{iH^{(0)}t}\eta^*(t)] = \sum_{k=1}^{N}\sum_{l=1}^{N} e^{i(E_l - E_k)t} \eta_k(t) \eta_l^*(t) \times \int dr\, \phi_m^*(r) \phi_l^*(r) \phi_k(r) \phi_n(r). \tag{38}$$

Here, we consider only the cases where either (i) $\varepsilon(t)$ is the control with g being a constant, or (ii) $g(t)$ is the control and $\varepsilon(t) = 0$. For these two scenarios, some general comments on mechanism can be made, under the assumption that the controls are of modest intensity, enabling the perturbation expansion above to form a qualitative picture to understand the results in Sec. VI. In scenario (i), an optimal field $\varepsilon(t)$ is expected to dominantly oscillate at frequencies $E_n - E_m$ corresponding to the transitions $m \leftrightarrow n$ allowed by the system, which can be seen from the first- and second-order contributions from $p^{(1)}$ in Eq. (36b) and $p_a^{(2)}$ in Eq. (37a). Additional frequency components are likely to be seen as well, due to interaction between the field and the nonlinear term in the second-order contributions from $p_b^{(2)}$ in Eq. (37b) and $p_c^{(2)}$ in Eq. (37c). In scenario (ii), it can be seen from $p_d^{(2)}$ in Eqs. (37d) and (38) that $g(t)$ should show frequency components at $E_n + E_k - E_l - E_m$ according to the transitions allowed by the elements of $M[\psi(t), \psi^*(t)]$. Additional complex spectral features can arise when power shifting occurs with strong controls.

The Dyson expansion can be useful in examining the structure of optimal controls, as we will show in Sec. VI. With the complexity of control over NLS dynamics, further mechanistic insights may be gained by an extension of the so-called Hamiltonian encoding technique [43], which is left to future study.

V. ALGORITHMS FOR LANDSCAPE EXPLORATION

This work uses the D-MORPH algorithm [30,31] to explore the control landscape. The algorithm parametrizes the control $c(t) \to c(t,s)$ with the continuous variable $s \geqslant 0$, and traversal of the landscape corresponds to a trajectory as a function of s, starting with an initial trial control $c(t,0)$. Suitable governing equations of $c(t,s)$ are derived in the following to enable (1) ascent and descent of the landscape, and (2) level-set exploration at the top. The analysis in step (2) could be performed as well at the bottom [27] (not shown here).

A. Ascent and descent algorithms

We present the governing equation of $c(t,s)$ for either landscape ascent or descent. Differentiating $P_{i\to f}(T,s)$ with respect to s yields

$$\frac{\partial P_{i\to f}}{\partial s} = \int_0^T dt\, \frac{\delta P_{i\to f}}{\delta c(t)} \frac{\partial c(t,s)}{\partial s}. \tag{39}$$

Ascent along the trajectory requires $\partial P_{i\to f}/\partial s \geqslant 0$, and descent requires $\partial P_{i\to f}/\partial s \leqslant 0$. Specifically, the ansatz

$$\frac{\partial c(t,s)}{\partial s} = \rho(s) \frac{\delta P_{i\to f}}{\delta c(t)} \tag{40}$$

with the choice $\rho(s) > 0$ guarantees that $\partial P_{i\to f}/\partial s \geqslant 0$, while $\rho(s) < 0$ similarly assures that $\partial P_{i\to f}/\partial s \leqslant 0$. The magnitude of $\rho(s)$ determines the rate of climbing. Equation (40) is a first-order D-MORPH differential equation, and was solved to find the control as a function of s using MATLAB's fourth-order Runge-Kutta solver ODE45, starting with an arbitrary trial control $c(t,0)$.

B. Level-set exploration algorithm

A governing equation for $c(t,s)$ is derived to give a trajectory along the level set at the top of the landscape, $P_{i\to f}(T) = 1$. At the top $\partial P_{i\to f}/\partial s = 0$, so that any change in $P_{i\to f}(T)$ comes from second-order contributions. Staying on the top therefore requires that $\partial^2 P_{i\to f}/\partial s^2 = 0$, with

$$\frac{\partial^2 P_{i\to f}}{\partial s^2} = \int_0^T dt\, \frac{\delta P_{i\to f}}{\delta c(t)} \frac{\partial^2 c(t,s)}{\partial s^2} + \frac{1}{2}\int_0^T dt' \int_0^T dt\, \frac{\partial c(t,s)}{\partial s} \frac{\delta^2 P_{i\to f}}{\delta c(t)\delta c(t')} \frac{\partial c(t',s)}{\partial s} = \frac{1}{2}\int_0^T dt' \int_0^T dt\, \frac{\partial c(t,s)}{\partial s} \frac{\delta^2 P_{i\to f}}{\delta c(t)\delta c(t')} \frac{\partial c(t',s)}{\partial s} = 0, \tag{41}$$

where the second step follows because $\delta P_{i\to f}/\delta c(t) = 0$ at the top for $t \in [0,T]$. Furthermore, as the Hessian $\delta^2 P_{i\to f}/\delta c(t)\delta c(t')$ at the top is a real symmetric matrix with

at most $2N-2$ nonzero eigenvalues (Sec. III B 2), it can be expressed as

$$\frac{\delta^2 P_{i\to f}}{\delta c(t)\delta c(t')} = \sum_{l=1}^{2N-2} \lambda_l \nu_l(t)\nu_l(t'), \tag{42}$$

where $\{\lambda_l\}$ for $l = 1,2,\ldots,2N-2$ are the nonzero eigenvalues of the Hessian and $\{\nu_l(t)\}$ the corresponding eigenfunctions, which form an orthonormal set, i.e., $\int_0^T dt\, \nu_k(t)\nu_l(t) = \delta_{kl}$. Using Eq. (42), the requirement for staying on the top in Eq. (41) becomes

$$\frac{\partial^2 P_{i\to f}}{\partial s^2} = \frac{1}{2}\sum_{l=1}^{2N-2} \lambda_l \left[\int_0^T dt\, \frac{\partial c(t,s)}{\partial s}\nu_l(t)\right]^2 = 0. \tag{43}$$

Equation (43) may only be satisfied if $\partial c(t,s)/\partial s$ has no projection in the space spanned by $\{\nu_l(t)\}$. To satisfy this requirement, the second-order D-MORPH level-set equation becomes

$$\frac{\partial c(t,s)}{\partial s} = \hat{P}\, h(t,s), \tag{44}$$

where $\hat{P}$ is specified by its action on the freely chosen function $h(t,s)$ such that

$$\hat{P}\, h(t,s) = h(t,s) - \sum_{l=1}^{2N-2} \nu_l(t) \int_0^T dt'\, \nu_l(t')h(t',s), \tag{45}$$

which projects $h(t,s)$ onto the null space of the Hessian. The second-order D-MORPH [Eq. (44)] is integrated using ODE45 in MATLAB, starting with the initial condition $c(t,0)$ as a field previously determined to give $P_{i\to f}(T) = 1$ by the algorithm in Sec. V A.

Although making an arbitrary choice for the function $h(t,s)$ permits free exploration of the level set at the top, $h(t,s)$ may also be chosen to maximize or minimize some auxiliary objective $F[c(t,s)]$, while maintaining $P_{i\to f}(T) = 1$. The change in the auxiliary objective $F[c(t,s)]$ along the level-set trajectory can be written using Eq. (44) as

$$\frac{\partial F}{\partial s} = \int_0^T dt\, \frac{\delta F}{\delta c(t)}\frac{\partial c(t,s)}{\partial s} = \int_0^T dt\, \frac{\delta F}{\delta c(t)}\, \hat{P}\, h(t,s). \tag{46}$$

Since the projection operator $\hat{P}$ is positive semidefinite, choosing $h(t,s) = \alpha(s)\delta F/\delta c(t)$ in Eq. (45) ensures that Eq. (46) is positive for $\alpha(s) > 0$ and negative for $\alpha(s) < 0$, respectively, maximizing and minimizing $F[c(t,s)]$ along the trajectory. A common auxiliary objective is to minimize the fluence of $\varepsilon(t)$, i.e.,

$$F[c(t,s)] = \int_0^T dt\, \varepsilon(t,s)^2, \tag{47}$$

which is treated in the simulations in Sec. VI by using $h(t,s) = 2\alpha(s)\varepsilon(t,s)$ with $\alpha(s) < 0$. Other auxiliary objectives may also be considered, such as maximization of robustness by minimizing the magnitude of the Hessian eigenvalues on a level-set trajectory [27].

In order to explore the level set at the top, Eq. (40) is employed first to maximize $P_{i\to f}(T)$ to an acceptable tolerance, taken in this work as $P_{i\to f}(T) = 1-\delta$, $\delta \leqslant 10^{-3}$. Solving Eq. (44) for a level-set trajectory can incur numerical errors leading to coming off the top [i.e., $P_{i\to f}(T) < 0.999$]. Whenever the latter event happens, the algorithm returns to Eq. (40) in an attempt to climb back up and then proceed with further integration of Eq. (44).

C. Gradient and Hessian of the objective

Equations (40) and (44) require evaluation of the gradient $\delta P_{i\to f}/\delta c(t)$ at any point on the landscape, as well as the Hessian $\delta^2 P_{i\to f}/\delta c(t)\delta c(t')$ at the top. Equations (13) and (28) show that the gradient and Hessian require knowledge of $|\delta\psi(T)/\delta c(t)\rangle$. To this end, the first-order variation in the state is derived in the following analysis; then, an efficient method of computing the gradient is presented.

1. *Objective variation*

The first variation of the NLS in Eq. (8) with respect to a change $\delta c(t)$ in the control is

$$\begin{aligned} i\frac{d}{dt}|\delta\psi(t)\rangle = {} & (H^{(0)} + H^{(1)}[\psi(t),\psi^*(t);\, c(t)])|\delta\psi(t)\rangle \\ & + (A^{(1)}[\psi(t),\psi^*(t);\, c(t)])|\delta\psi(t)\rangle \\ & + (B^{(1)}[\psi(t),\psi^*(t);\, c(t)])|\delta\psi^*(t)\rangle \\ & + \left(\frac{\delta}{\delta c(t)}H^{(1)}[\psi(t),\psi^*(t);\, c(t)]\right)\delta c(t)|\psi(t)\rangle. \end{aligned} \tag{48}$$

The matrices $A^{(1)}[\psi(t),\psi^*(t);\, c(t)]$ and $B^{(1)}[\psi(t),\psi^*(t);\, c(t)]$ have the following elements:

$$\begin{aligned} A^{(1)}_{ji}[\psi(t),\psi^*(t);\, c(t)] = {} & \sum_{m=1}^{N}\psi_m(t)\int dr\, \phi_j^*(r) \\ & \times\left(\frac{\delta}{\delta\psi}\hat{H}^{(1)}[\psi(r,t),\psi^*(r,t);\, c(t)]\right) \\ & \times \phi_m(r)\phi_i(r), \end{aligned} \tag{49a}$$

$$\begin{aligned} & B^{(1)}_{ji}[\psi(t),\psi^*(t);\, c(t)] \\ & = \sum_{n=1}^{N}\psi_n(t)\int dr\, \phi_j^*(r)\phi_i^*(r) \\ & \quad\times\left(\frac{\delta}{\delta\psi^*}\hat{H}^{(1)}[\psi(r,t),\psi^*(r,t);\, c(t)]\right)\phi_n(r), \end{aligned} \tag{49b}$$

where $\frac{\delta}{\delta\psi}$ denotes the partial functional derivative with respect to $\psi(r,t)$, and analogously for $\frac{\delta}{\delta\psi^*}$. Note that through the nonlinear term both $|\delta\psi(t)\rangle$ and $|\delta\psi^*(t)\rangle$ enter Eq. (48), leading to a set of coupled equations for these variations. As both $|\delta\psi(t)\rangle$ and $|\delta\psi^*(t)\rangle$ are length-N column vectors, the coupled equations may be expressed together in supermatrix form

$$\begin{aligned} i\frac{d}{dt}\delta z(t) = {} & L(t)\delta z(t) \\ & + \delta c(t)\begin{bmatrix} \left(\frac{\delta}{\delta c(t)}H^{(1)}\right) & \emptyset \\ \emptyset & -\left(\frac{\delta}{\delta c(t)}H^{(1)}\right)^* \end{bmatrix} z(t), \end{aligned} \tag{50}$$

with initial condition $\delta z(0) = 0$, where the length-$2N$ column supervector $z(t)$ is

$$z(t) \equiv \frac{1}{\sqrt{2}}\begin{bmatrix} |\psi(t)\rangle \\ |\psi^*(t)\rangle \end{bmatrix}, \tag{51}$$

and similarly for $\delta z(t)$. In Eq. (50), $\emptyset$ denotes the $N \times N$ zero matrix, and $L(t)$ is a $2N \times 2N$ supermatrix

$$L(t) = \begin{bmatrix} H^{(0)} + H^{(1)} + A^{(1)} & B^{(1)} \\ -(B^{(1)})^* & -(H^{(0)} + H^{(1)} + A^{(1)})^* \end{bmatrix}, \tag{52}$$

introducing the compact notation $H^{(1)} \equiv H^{(1)}[\psi(t),\psi^*(t);\ c(t)]$, $A^{(1)} \equiv A^{(1)}[\psi(t),\psi^*(t);\ c(t)]$, and $B^{(1)} \equiv B^{(1)}[\psi(t),\psi^*(t);\ c(t)]$.

Equation (50) can be solved by introducing a Green's function $G(t,t')$, $t \geqslant t'$, satisfying

$$i\frac{\partial}{\partial t}G(t,t') = L(t)G(t,t'), \quad G(t',t') = \mathbf{I}. \tag{53}$$

Using Eq. (53), the solution to Eq. (50) at final time T can be expressed as

$$\delta z(T) = -i\int_0^T dt\, \delta c(t)\, G(T,t) \times \begin{bmatrix} \left(\frac{\delta}{\delta c(t)}H^{(1)}\right) & \emptyset \\ \emptyset & -\left(\frac{\delta}{\delta c(t)}H^{(1)}\right)^* \end{bmatrix} z(t), \tag{54}$$

which yields the relation

$$\frac{\delta}{\delta c(t)}z(T) = -iG(T,t)\begin{bmatrix} \frac{\delta}{\delta c(t)}H^{(1)} & \emptyset \\ \emptyset & -\left(\frac{\delta}{\delta c(t)}H^{(1)}\right)^* \end{bmatrix} z(t). \tag{55}$$

Substituting Eq. (55) for $\delta z(T)/\delta c(t)$ into Eq. (13), the first derivative of the cost functional with respect to $c(t)$ is

$$\frac{\delta P_{i\to f}}{\delta c(t)} = -iz^\dagger(T)\,\mathbf{O}\,G(T,t) \times \begin{bmatrix} \frac{\delta}{\delta c(t)}H^{(1)} & \emptyset \\ \emptyset & -\left(\frac{\delta}{\delta c(t)}H^{(1)}\right)^* \end{bmatrix} z(t), \tag{56}$$

where $z^\dagger(T)$ is the conjugate transpose of $z(T)$ and the $2N \times 2N$ supermatrix $\mathbf{O}$ is

$$\mathbf{O} \equiv \begin{bmatrix} |\phi_f\rangle\langle\phi_f| & \emptyset \\ \emptyset & |\phi_f^*\rangle\langle\phi_f^*| \end{bmatrix}. \tag{57}$$

Similarly, the Hessian at the top is found by substituting Eq. (55) into (28), yielding

$$\frac{\delta^2 P_{i\to f}}{\delta c(t)\delta c(t')} = -2z^\dagger(t')\begin{bmatrix} \frac{\delta}{\delta c(t')}H^{(1)} & \emptyset \\ \emptyset & -\left(\frac{\delta}{\delta c(t')}H^{(1)}\right)^* \end{bmatrix} G^\dagger(T,t')\,(\mathbf{O}-\mathbf{I})\,G(T,t) \begin{bmatrix} \frac{\delta}{\delta c(t)}H^{(1)} & \emptyset \\ \emptyset & -\left(\frac{\delta}{\delta c(t)}H^{(1)}\right)^* \end{bmatrix} z(t). \tag{58}$$

For the particular case of the GPE, explicit expressions for the gradient with respect to the control, either $\varepsilon(t)$ or $g(t)$, are found by substitution of $H^{(1)} = -\mu\varepsilon(t) + g(t)M[\psi(t),\psi^*(t)]$ into the variational equations, giving

$$\frac{\delta P_{i\to f}}{\delta \varepsilon(t)} = -iz^\dagger(T)\,\mathbf{O}\,G(T,t)\begin{bmatrix} -\mu & \emptyset \\ \emptyset & \mu^* \end{bmatrix} z(t), \tag{59a}$$

$$\frac{\delta P_{i\to f}}{\delta g(t)} = -iz^\dagger(T)\,\mathbf{O}\,G(T,t)\begin{bmatrix} M[\psi(t),\psi^*(t)] & \emptyset \\ \emptyset & -M[\psi(t),\psi^*(t)] \end{bmatrix} z(t), \tag{59b}$$

where $G(T,t)$ is the Green's function driven by $L(t)$, which [cf. Eq. (52)] becomes

$$L(t) = \begin{bmatrix} H^{(0)} - \mu\varepsilon(t) + 2g(t)M[\psi(t),\psi^*(t)] & g(t)M[\psi(t),\psi(t)] \\ -g(t)M[\psi^*(t),\psi^*(t)] & -\Big(H^{(0)} - \mu\varepsilon(t) + 2g(t)M[\psi(t),\psi^*(t)]\Big)^* \end{bmatrix}. \tag{60}$$

Similarly, expressions for the Hessian at the top with respect to $\varepsilon(t)$ and $g(t)$ for the GPE are

$$\frac{\delta^2 P_{i\to f}}{\delta \varepsilon(t)\delta\varepsilon(t')} = -2z^\dagger(t')\begin{bmatrix} -\mu & \emptyset \\ \emptyset & \mu^* \end{bmatrix} G^\dagger(T,t')\,(\mathbf{O}-\mathbf{I})\,G(T,t) \times \begin{bmatrix} -\mu & \emptyset \\ \emptyset & \mu^* \end{bmatrix} z(t), \tag{61a}$$

$$\frac{\delta^2 P_{i\to f}}{\delta g(t)\delta g(t')} = -2z^\dagger(t')\begin{bmatrix} M[\psi(t),\psi^*(t)] & \emptyset \\ \emptyset & -M[\psi(t),\psi^*(t)] \end{bmatrix} \times G^\dagger(T,t')(\mathbf{O}-\mathbf{I})G(T,t) \times \begin{bmatrix} M[\psi(t),\psi^*(t)] & \emptyset \\ \emptyset & -M[\psi(t),\psi^*(t)] \end{bmatrix} z(t). \tag{61b}$$

Equations (59a) and (59b) may be used in ascent and descent of the landscape, while Eqs. (61a) and (61b) allow for level-set exploration at the top.

2. *Adjoint method for gradient evaluation*

For computational efficiency, the gradient in Eq. (13) is rewritten as

$$\frac{\delta P_{i\to f}}{\delta c(t)} = -2i\,\chi(t)\begin{bmatrix} \frac{\delta}{\delta c(t)}H^{(1)} & \emptyset \\ \emptyset & -\left(\frac{\delta}{\delta c(t)}H^{(1)}\right)^{*}\end{bmatrix} z(t),$$
$$\chi(t) = z^{\dagger}(T)\,\mathbf{O}\,G(T,t), \tag{62}$$

where $\chi(t)$ can be efficiently found using backward integration of the adjoint equation [44]

$$\frac{d}{dt}\chi(t) = z^{\dagger}(T)\,\mathbf{O}\,\frac{\partial}{\partial t}G(T,t)$$
$$= i\,\chi(t)L(t), \tag{63}$$

with the final condition $\chi(T) = z^{\dagger}(T)\mathbf{O}$. Backward integration of $\chi(t)$ is more efficient than forward integration of $G(T,t)$, as $\chi(t)$ is a length-$2N$ vector and $G(T,t)$ is a $2N \times 2N$ matrix. Equation (63) is integrated using a simple second-order Runge-Kutta method, which was significantly faster than methods such as MATLAB's ODE45 or ODE23 solvers and showed negligible loss of accuracy. While $G(T,t)$ is never explicitly computed for the gradient, it is still necessary for computation of $\delta z(t)/\delta c(t)$ and thus for evaluation of the Hessian using Eq. (28). The state $z(t)$ is computed with matrix exponentiation over sufficiently small time steps, using MATLAB's EXPM method.

In actually testing the results of the Hessian predicted by Eqs. (23) and (28), finite differences for the Hessian will be employed in Secs. VI A 2 and VI A 3, respectively. However, when moving along the top-level set, Eq. (44) will be employed by utilizing Eq. (28).

VI. NUMERICAL SIMULATIONS

This section presents control simulations with the N-level GPE in Eq. (9), using dimensionless units for all variables. For simplicity, the basis set $\{\phi_n(r)\}$ is taken to be real, making $M[\psi(t),\psi^*(t)]$ in Eq. (11) a symmetric square matrix. In particular, the basis members are the eigenfunctions $\phi_n(r) = \sqrt{\frac{2}{L}}\sin(\frac{n\pi r}{L})$ of $\hat{H}^{(0)}$ for a particle in a box of size $L = \pi$ or 2π, noting that model BECs have been studied in such traps [45]. In most of the simulations, the initial and final states $|\phi_i\rangle$ and $|\phi_f\rangle$ are taken as eigenfunctions of $\hat{H}^{(0)}$, although superpositions of $\{|\phi_n\rangle\}$ are also considered for illustration. In addition, for numerical stability reasons, the magnitude of g considered here is modest, on the same order of magnitude as the energy-level spacings in $H^{(0)}$.

Two control schemes are considered for the GPE. In the first, $c(t) = \varepsilon(t)$ with $H^{(1)} = -\mu\varepsilon(t) + gM[\psi(t),\psi^*(t)]$, and the coefficient of the nonlinear term g is constant. In the second scenario, $c(t) = g(t)$ with $H^{(1)} = g(t)M[\psi(t),\psi^*(t)]$, and the electric field is not present. The simulations primarily focus on control with the field $\varepsilon(t)$ in Sec. VI A, and a select number of simulations are shown with $g(t)$ in Sec. VI B.

A. Electric field control

1. *Climbing to the landscape top*

The landscape analysis of Sec. III predicts that no suboptimal traps should exist upon satisfaction of the three assumptions set out in Sec. I. In order to assess the validity of this finding, over 800 simulations were conducted with a variety of systems and initial fields. The first-order D-MORPH equation [Eq. (40)] was solved to climb the landscape, and in all cases $P_{i\to f}(T,s)$ increased monotonically in s until the simulations were stopped upon reaching a value of $s_{\max}$ at which $P_{i\to f}(T,s_{\max}) \geqslant 0.99$. The results are summarized in Table I. To excite a transition from $|\phi_i\rangle$ to $|\phi_f\rangle$, it is natural to choose an initial field with components at the dipole-allowed transition frequencies of the system. Such initial fields often produced trajectories that reached the top quickly. We also considered control cases with poor initial guesses such as a constant field, a field oscillating at a high frequency (i.e., at $2\omega_{\max}$, where $\omega_{\max}$ was the highest dipole-allowed transition frequency), or a field oscillating at a dipole-forbidden transition frequency. In all cases, summarized in Table I, full control to $P_{i\to f}(T) \geqslant 0.99$ was achieved, verifying the validity of the assumptions in Sec. I leading to the trap-free landscape conclusion of Sec. III.

For illustration, the results for an $N = 10$ case are presented here. The system models a particle in a box with $L = 2\pi$, and $g = 1$. The transition dipole has nearest-neighbor coupling ($\mu_{i,i+1} = \mu_{i+1,i} = 1.0$) and weaker next-nearest-neighbor coupling ($\mu_{i,i+2} = \mu_{i+2,i} = 0.5$). The lowest allowed transition frequency is $\omega_{1\leftrightarrow 2} = 0.375$, and we set $T = 40$ for adequate resolution of the transition. The goal is to maximize the $1 \to 10$ transition probability. The initial field in Fig. 1(a) has frequency components at most of the nearest-neighbor transitions. The initial field produced a small yield of only $P_{1\to 10} = 0.01$, and the optimal field in Fig. 1(a) created a yield $P_{1\to 10} = 0.99$. The power spectra of the initial and optimal fields are shown in Fig. 1(b), where a small dc component is seen in the optimal field. The initial field has a narrow bandwidth, while the optimal field has frequencies corresponding to all of the dipole-allowed transitions thereby exploiting multiple pathways to the target state; additional

TABLE I. Results for electric field control

System					Optimization	
Levels	μ[a]	g[b]	L	Targets	Yield	Runs
3	All allowed, or one disallowed	$0.1-2$ (+ or −)	π	$1\to 2$ $1\to 3$ $1\to$ s.p.[c]	0 99[d]	800
5	All allowed, or nearest neighbor	$0.5-2$ (+ or −)	π	$1\to 2$ $1\to 5$	0 99	25
7	Nearest and next-nearest neighbor	+1	π	$1\to 7$	0 99	2
10	Nearest and next-nearest neighbor	+1	2π	$1\to 10$	0 99	4

[a]Dipole selection rules.
[b]Signs are those of g.
[c]s.p. means superposition state.
[d]Select cases taken up to a precision of $10^{-5} \sim 10^{-6}$.

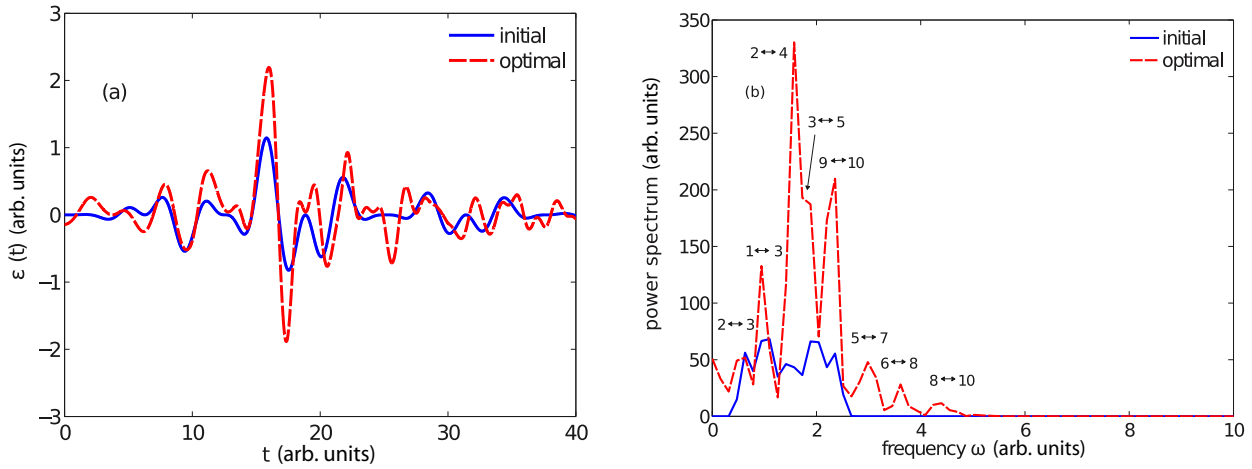

FIG. 1. (Color online) A 10-level system with the goal of maximizing the $1 \rightarrow 10$ transition probability with electric field control. (a) The initial field (solid line), which gave a yield of $P_{1\rightarrow 10}(T) = 0.01$, resonates at many of the allowed transitions, and has the form $\varepsilon(t,0) = 2\ \exp[-\frac{4\pi}{T^2}(t - T/2)^2]\sin(1.5t)\sin(0.5t)\sin(0.25t)\sin(0.125t)$. The optimal field (dashed line) $\varepsilon(t,s_{\max})$ gave a yield of $P_{i\rightarrow f}(T) = 0.99$. (b) The power spectra of the initial (solid line) and final (dashed line) fields with some of the allowed dipole transitions indicated.

frequency components are likely also present through higher-order contributions from the nonlinear terms in the expansion in Eq. (34). Although the complicated nature of the optimal field makes it difficult to fully discern the mechanism of the excitation, the level populations $P_{1\rightarrow j}(t)$ over time in Fig. 2 indicate mainly a nearest- and next-nearest-neighbor climbing mechanism allowed by the dipole couplings, although the detailed features in the curves suggest that additional dynamics is involved.

2. *Hessian at the landscape bottom*

Assessment of the Hessian at the bottom of the landscape is important for verifying the theoretical predictions in Sec. III,

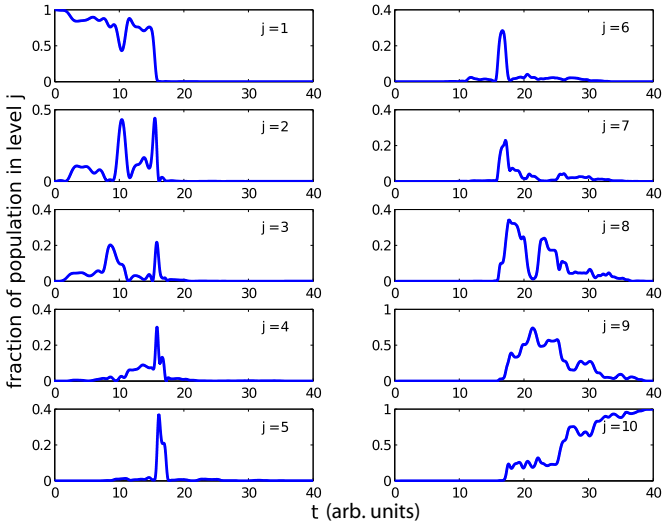

FIG. 2. (Color online) Populations over time for the $1 \rightarrow j$ transitions in the 10-level system in Fig. 1. Population dynamics suggest mainly a ladder-climbing mechanism, with a sharp transition occurring at $t \approx 17$ in accord with the strongest part of the control pulse in Fig. 1(a).

and the nature of the Hessian there is particularly relevant for initial fields producing low yields $P_{i\rightarrow f}(T) \approx 0$. For the linear Schrödinger equation, the trivial control $\varepsilon(t) = 0$ with $\langle \phi_f \mid \phi_i \rangle = 0$ will correspond to a point at the bottom of the landscape $P_{i\rightarrow f}(T) = 0$. However, $\varepsilon(t) = 0$ generally will produce $P_{i\rightarrow f}(T) > 0$ due to the nonlinear term in the NLS. Thus, we performed a gradient descent to find a nontrivial field producing $P_{i\rightarrow f}(T) = 0$. The resultant Hessian was diagonalized at the bottom of the landscape, and a Fourier analysis of the eigenvectors was employed to reveal the structure of control variations as a function of frequency that could best lift $P_{i\rightarrow f}(T)$ off the landscape bottom. The Hessian $\delta^2 P_{i\rightarrow f}(T)/\delta c(t)\delta c(t')$ is real, symmetric, with eigenvectors being real functions of time; the eigenvectors are complex functions of frequency, so their power spectra are reported in the analysis below.

As an illustration, we consider a three-level particle-in-a-box system with $L = \pi$ and $g = 1$, with $H^{(0)}$ having energy levels $E_1 = 0.5$, $E_2 = 2.0$, and $E_3 = 4.5$. Although the full Hamiltonian $H(t) = H^{(0)} + H^{(1)}[\psi(t),\psi^*(t); c(t)]$ is time dependent, diagonalization of $H(t)$ at selected times is valuable for providing insight regarding power shifting of the transition frequencies. The energy levels obtained from diagonalizing $H^{(0)} - \mu\varepsilon(t) + gM[\psi(t),\psi^*(t)]$ at various values of t shift in approximately a coordinated fashion (not shown), so that the transition frequencies of the nonlinear Hamiltonian are not noticeably different from that of $H^{(0)}$, including frequencies $\omega_{1\leftrightarrow 2} = 1.5, \omega_{2\leftrightarrow 3} = 2.5$, and $\omega_{1\leftrightarrow 3} = 4$. All dipole transitions are allowed, with the target transition being $P_{1\rightarrow 3}(T)$, and $T = 10$ is sufficient for spectral resolution. The trial field is $\varepsilon(t) = 0.25\sin(4t)$ and gradient descent was used with Eq. (40), $\rho(s) = -1$, to find a nontrivial control (not shown) that produced a final yield of $P_{1\rightarrow 3}(T) \approx 10^{-13}$. The Hessian in Eq. (23) is predicted to have a rank of at most two, and this result was verified using a finite-difference calculation of the Hessian at the bottom of the landscape with $dt = 0.02$ and $\delta\varepsilon = 0.001$, chosen small enough to provide convergence. Figure 3 shows the first 20 eigenvalues of the Hessian,

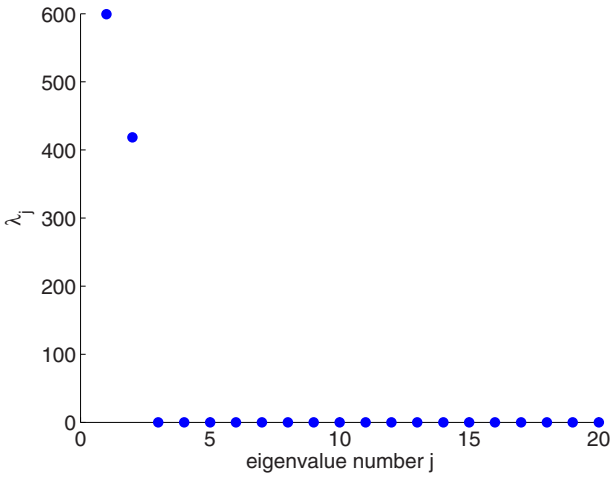

FIG. 3. (Color online) First 20 eigenvalues of the Hessian at the bottom of the landscape for a three-level system with electric field control. Two nonzero eigenvalues are evident, and all remaining eigenvalues are negligible. The magnitude of these two nonzero eigenvalues indicates that variations of ∼1% in the control that follow either of the first two eigenvectors at the bottom are expected to increase the yield by $\delta P_{i\to f} \sim 0.05$.

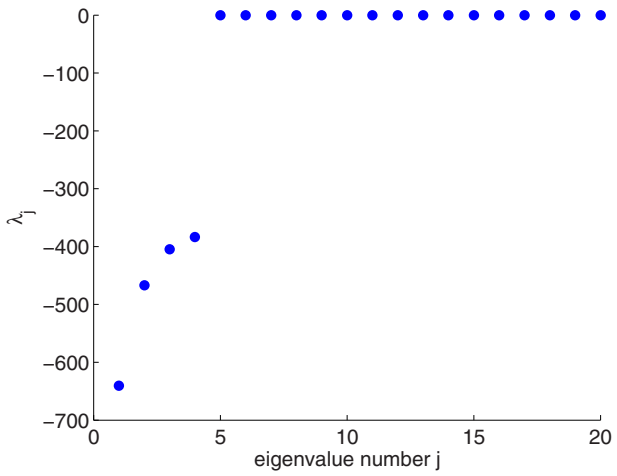

FIG. 5. (Color online) First 20 eigenvalues of the Hessian at the top of the landscape for a three-level system with electric field control. As predicted for the top of the landscape, there are $2N-2=4$ nonzero eigenvalues, and the remaining eigenvalues are negligible. The magnitudes of the nonzero eigenvalues indicate that variations of ∼ % in the control specified by either of the first four eigenvectors are expected to decrease the yield by $\delta P_{i\to f} \sim 0.05$.

with the remaining eigenvalues essentially being zero. Two nonzero eigenvalues are evident, consistent with the rank-two conclusion in Sec. III.

Power spectra of select eigenvectors of the Hessian at the bottom are shown in Fig. 4. Both eigenvectors associated with the nonzero eigenvalues in Figs. 4(a) and 4(b) have strong frequency components near $\omega_{1\leftrightarrow 3}=4$. Because the field at the bottom of the landscape produces a final state with 0.941 population in $|\phi_1\rangle$ and 0.059 population in $|\phi_2\rangle$, these results are consistent with the largest increase in $P_{i\to f}(T)$ coming from a $1\to 3$ mechanism to most effectively lift off the landscape bottom. Figure 4(c) shows the power spectra of select eigenvectors in the null space of the Hessian at the landscape bottom. In the null space, many of the contributions in the power spectra lie outside the direct transition frequency range of the system (i.e., $\omega<4$). This result is intuitive, but what is surprising is that the third and tenth eigenvectors (solid and dashed lines, respectively) as an illustration have significant contribution from frequencies corresponding to dipole-allowed transitions in the system, including $\omega_{1\leftrightarrow 2}=1.5$ and $\omega_{2\leftrightarrow 3}=2.5$. The coordinated disturbance reflecting these eigenvectors likely excites multiple transition pathways in the expansion in Eqs. (36b) and (36c) and even higher-order terms, where $\varepsilon(t)$ now refers to the nontrivial control at the bottom with an additional small perturbation along the null-space eigenvectors. The unusual frequency structure in the null-space eigenvectors may thereby produce destructive interference between said pathways, leaving $P_{1\to 3}(T)\approx 0$. All of the plots in Fig. 4 show frequencies distinct from simply $\{\omega_{i\leftrightarrow j}\}$ [e.g., in Fig. 4(a) the peak is slightly shifted away from $\omega_{1\leftrightarrow 3}=4$], likely reflecting the nonlinear contributions in the expansion in Eqs. (36b) and (36c), including possibly from $\eta(t)$.

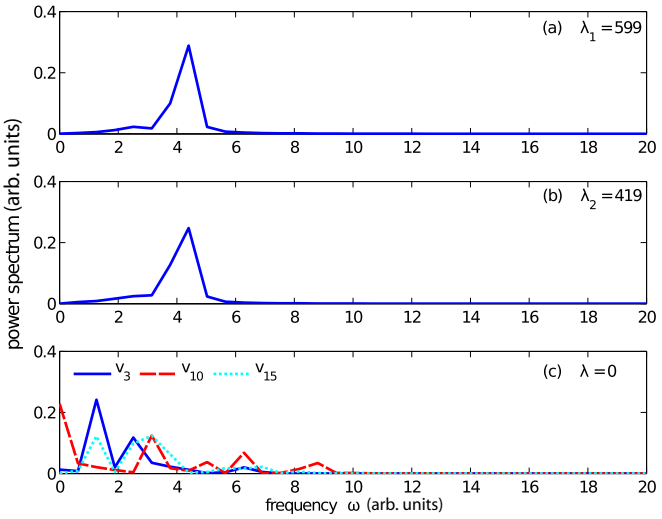

FIG. 4. (Color online) Power spectra of selected eigenvectors of the Hessian at the bottom of the landscape for the three-level system in Fig. 3. Panels (a) and (b) show the two eigenvectors of the Hessian with nonzero eigenvalues, where the major contribution is near $\omega_{1\leftrightarrow 3}=4$. Note that the eigenvector power spectra are shown, and the actual eigenvectors are orthonormal. Panel (c) shows eigenvectors 3, 10, and 15, all in the null space with $\lambda=0$. The null space contains a range of frequency components in addition to $\omega_{1\leftrightarrow 2}=1.5$ and $\omega_{2\leftrightarrow 3}=2.5$.

3. *Hessian at the landscape top*

The Hessian is also calculated at the landscape top to further assess the rank-analysis predictions of Sec. III. As an illustration, for the same system in Sec. VI A 2, the first-order D-MORPH technique in Eq. (40) is employed with $\rho(s)=+1$ to find an optimal field at the top. The Hessian in the landscape analysis in Eq. (28) is predicted to have rank at most $2N-2$, and the validity of this result was assessed using a finite-difference calculation of the Hessian at the top

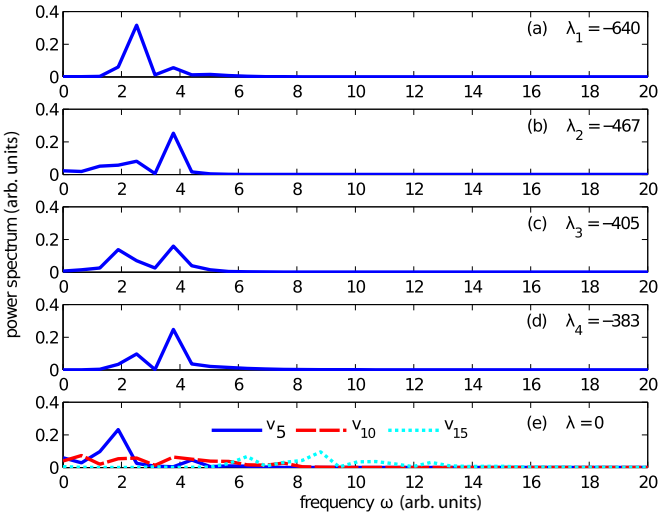

FIG. 6. (Color online) Power spectra of selected eigenvectors of the Hessian at the top of the landscape for the three-level system in Fig. 5. Panels (a)−(d) show the four eigenvectors of the Hessian with nonzero eigenvalues; significant frequency components occur at $\omega_{2\leftrightarrow3} = 2.5$, $\omega_{1\leftrightarrow3} = 4$, and, to a lesser degree, $\omega_{1\leftrightarrow2} = 1.5$. The last plot (e) shows eigenvectors 5, 10, and 15, all in the null space, with a wide range of higher-frequency components. In addition, eigenvector 5 has significant overlap with the $\omega_{1\leftrightarrow2} = 1.5$ transition frequency.

of the landscape with $dt = 0.02$ and $\delta\varepsilon = 0.001$. Figure 5 shows the first 20 eigenvalues of the Hessian at the top, with the remaining eigenvalues essentially being zero. The evident four nonzero eigenvalues are consistent with the Hessian rank analysis in Sec. III of $2N - 2 = 4$.

The power spectra of select eigenvectors of the Hessian at the top are also shown in Fig. 6. The first four eigenvectors in Figs. 6(a)–6(d) display peaks that overlap with the transitions $\omega_{2\leftrightarrow3} = 2.5$, $\omega_{1\leftrightarrow3} = 4$, and to a lesser degree, $\omega_{1\leftrightarrow2} = 1.5$. This result has the intuitive interpretation that variations around these system transition frequencies would maximally reduce population in the target state $|\phi_3\rangle$. Figure 6(e) shows the power spectra of select eigenvectors in the null space of the Hessian at the top. As with Fig. 4 for the Hessian null space on the landscape bottom, the eigenvectors in the null space at the top show a range of spectral components beyond the allowed frequency range of the Hamiltonian (i.e., neglecting nonlinear contributions). A surprising result is that the fifth eigenvector (solid line), in the null space, shows a peak centered at $\omega = 2$, with intensity at $\omega_{1\leftrightarrow2} = 1.5$ and to a lesser degree at $\omega_{2\leftrightarrow3} = 2.5$. It is likely that the corresponding induced transition pathways in Eqs. (36a)–(36c), and even higher-order terms, interfere destructively to preserve the value of $P_{i\to f}(T) \approx 1$ at the top of the landscape.

4. *Exploring the landscape top*

We now demonstrate level-set exploration at the top of the landscape using the second-order D-MORPH procedure in Eq. (44) [27], utilizing the Hessian calculated with Eq. (28), for the same system as in Secs. VI A 2 and VI A 3. The initial field $\varepsilon_1(t)$ produced a yield of $P_{1\to3}(T) = 0.999\,999$ to assure that the Hessian dominates the landscape behavior, and the level-set exploration is guided by minimizing the fluence $F[\varepsilon(t)]$ in Eq. (47). The initial optimal field $\varepsilon_1(t)$ with fluence $F[\varepsilon_1(t)] = 283$ is shown in Fig. 7(a) (solid line). The second-order D-MORPH procedure discovered a new optimal field $\varepsilon_2(t)$ with a significantly reduced fluence of $F[\varepsilon_2(t)] = 113$, shown as the dashed line in Fig. 7(a). The corresponding power spectra are plotted in Fig. 7(b) for comparison. While the difference between the two fields is quite pronounced, they both show strong contributions around the frequencies $\omega_{1\leftrightarrow2} = 1.5$ and $\omega_{2\leftrightarrow3} = 2.5$. The first optimal field $\varepsilon_1(t)$ also shows a strong contribution at $\omega_{1\leftrightarrow3} = 4$, suggesting that $1 \to 3$ is a dominant pathway, while the second optimal field $\varepsilon_2(t)$ is centered about $\omega_{1\leftrightarrow2} = 1.5$ and $\omega_{2\leftrightarrow3} = 2.5$, suggesting the mechanism $1 \to 2 \to 3$.

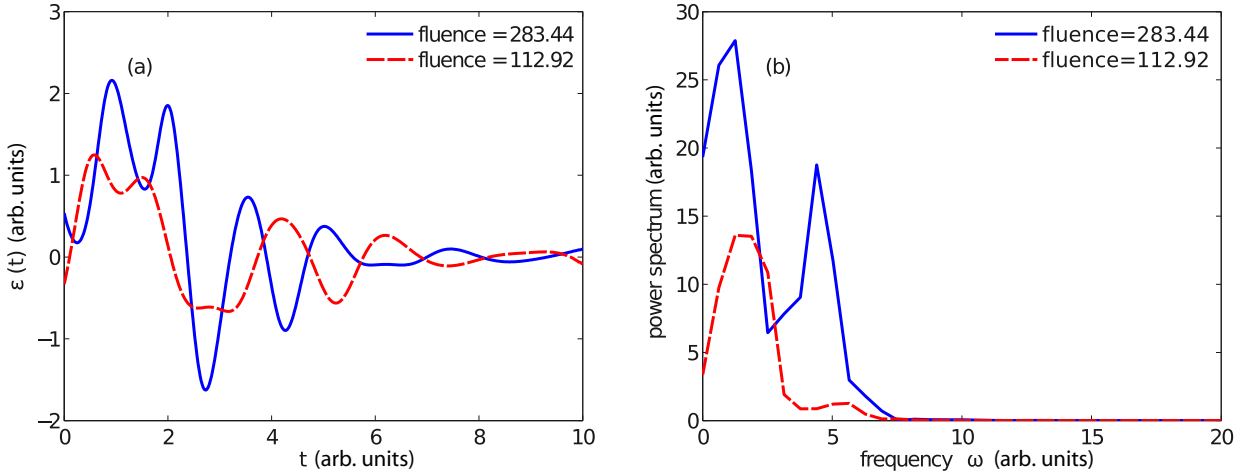

FIG. 7. (Color online) Exploration of the top of the landscape with the auxiliary objective of minimizing the fluence $F[\varepsilon(t)]$ in Eq. (47). (a) Initial field (solid line) and final field (dashed line) with their indicated fluence values for a three-level system with all allowed dipole transitions. Throughout the exploration, the fields on the top of the landscape gave a yield of $P_{1\to3}(T) > 0.999$. (b) The associated field power spectra.

TABLE II. Results for control with $g(t)$.

System			Optimization	
Levels	L	Targets	Yield	Runs
3	π	$1 \to 3$ s.p.[a]$\to 2$ s.p. $\to 3$	0.99	40

[a]s.p. means superposition state.

B. Nonlinear coupling coefficient control

We now explore the capability of only using $g(t)$ driving the nonlinear term as a control. The numerical calculations seek to assess whether the assumptions of Sec. I are adequately satisfied in this circumstance to draw the landscape conclusions in Sec. III. In particular, the target transition needs to satisfy assumption (i) that $|\phi_f\rangle$ is reachable from $|\phi_i\rangle$. No procedure is available to assess general satisfaction of assumption (i). While it is easy to construct pathological cases in violation of this assumption, this feature is not unique to the NLS; for example, it is also easy to construct a dipole and target transition $|\phi_i\rangle \to |\phi_f\rangle$ that violate the same assumption for the linear Schrödinger equation.

The simulations with $g(t)$ as a control considered three-level particle-in-a-box model systems, and the results are summarized in Table II. As an observed general trend, various combinations of transition frequencies in $H^{(0)}$ were found in each optimal control $g(t)$, attributed to the interaction of $g(t)$ with the nonlinear term $|\psi(r,t)|^2$ in the NLS (Sec. IV). Strong dc components were also evident. All the cases in Table II reached the top of the landscape with $P_{i\to f}(T) \geqslant 0.99$, verifying that the assumptions behind the landscape analysis are adequately satisfied.

A particular case illustrating the use of $g(t)$ as a control is shown in Fig. 8 for target transition $1 \to 3$ ($\omega_{1\leftrightarrow 3} = 4$). The optimization trajectory reached the top of the landscape, producing a yield of $P_{i\to f}(T) = 0.99$. For this case and choice of basis, $M[\psi(t),\psi^*(t)]$ has a special structure that decouples $|\phi_2\rangle$ from $|\phi_1\rangle$ and $|\phi_3\rangle$; in particular, with $|\psi(0)\rangle = [1;0;0]$, the nonlinear term at time $t = 0$ is

$$M[\psi(0),\psi^*(0)] = \begin{bmatrix} 0.477 & 0 & -0.159 \\ 0 & 0.318 & 0 \\ -0.159 & 0 & 0.318 \end{bmatrix}, \quad (64)$$

whose sparse structure is preserved throughout the subsequent time evolution. Thus, this case reduces to an effective two-level system. As a result of the coupling structure of the nonlinear term $M[\psi(t),\psi^*(t)]$ and the analysis of Sec. IV, the control $g(t)$ is expected to have frequencies $E_n + E_k - E_l - E_m$ for $k,l,m,n = 1,3$. In particular, this behavior results in contributions from frequencies $\omega_{1\leftrightarrow 3} = 4$ and $2\omega_{1\leftrightarrow 3} = 8$ shown in Fig. 8(b).

VII. CONCLUSIONS

This work is motivated by the significant interest in the NLS in several domains and the natural desire to control the associated dynamics. In particular, we sought to assess whether the control landscape for nonlinear quantum dynamics shared the very attractive features found for linear quantum dynamics [25,26]. To this end, this work examines optimal control of nonlinear quantum dynamics expressed with finite-level systems, where the physical objective is the maximization of $P_{i\to f}(T)$. It is shown that under three basic assumptions [i.e., (i) $|\phi_f\rangle$ is reachable from $|\phi_i\rangle$, (ii) the mapping $\delta c(t) \to |\delta\psi(T)\rangle$ is surjective, and (iii) the controls are unconstrained], the control landscape for nonlinear quantum dynamics is expected to be trap free. Thus, a myopic local gradient-climbing algorithm should be able to discover an optimal control $c(t)$ that can fully achieve the desired $|\phi_i\rangle \to |\phi_f\rangle$ transition. Furthermore, the landscape has a simple structure at the top and bottom, with the Hessian possessing finite rank and an infinite-dimensional null space. This quality enables level-set exploration for maximization or minimization of auxiliary physical objectives important in laboratory settings, and the presence of the Hessian null space indicates that

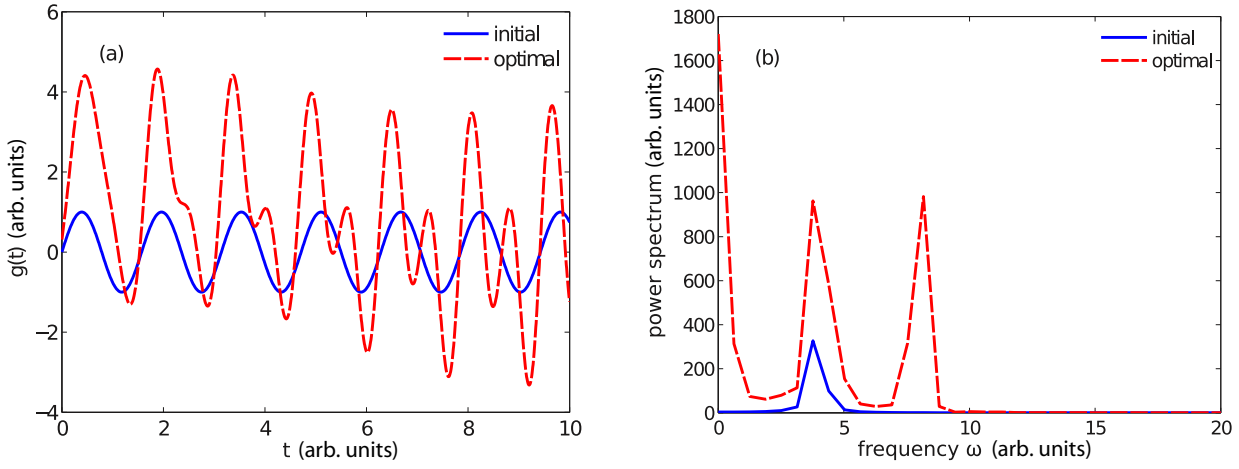

FIG. 8. (Color online) Simulation with $g(t)$ as the control for a three-level system. (a) The initial control $g(t) = \sin(4t)$ gave a yield of $P_{1\to 3}(T) = 0.40$ and the optimal $g(t)$ produced a yield of $P_{i\to f}(T) = 0.99$. (b) The power spectra of the initial and optimal controls. The optimal control has a strong dc feature along with a component at $\omega = \omega_{1\leftrightarrow 3} = 4$. The strong doubled-frequency component at $\omega = 2\omega_{1\leftrightarrow 3} = 8$ arises from the structure of the nonlinear term in the GPE.

optimal control solutions may have an inherent degree of robustness to noise. These findings for control of the NLS fully coincide with the previous landscape analysis for the linear Schrödinger equation [25,26,29].

Importantly, it is difficult to *a priori* assess whether the assumptions should be satisfied for any particular application. Thus, in parallel to the landscape analysis, we also present extensive numerical simulations on the GPE expanded in a particle-in-a-box basis for up to $N = 10$. All simulations reached $P_{i\to f}(T) \geqslant 0.99$ to provide numerical validation of the trap-free landscape conclusion, suggesting that it is not difficult to satisfy the three basic assumptions. Simulations also demonstrated the feasibility of level-set exploration at the top of the landscape, which may be used to find physically attractive controls.

While the success found in the numerical simulations suggests that the assumptions in the landscape analysis will hold in practice, further research is needed to explore the conditions when the assumptions are not adequately satisfied. Analytical tools need to be developed to identify the required structure of the Hamiltonian operators to assure state-to-state reachability for assumption (i). In the case of assumption (ii), an assessment is needed for the existence of nontrivial singular controls that violate the full rank of $\delta\psi(T)/\delta c(t)$; the added complexity of the nonlinear dynamics may aid in satisfying the full-rank condition. In addition, the presence of strong nonlinearities calls for due caution when limiting the number of basis functions or spatial grid points [18] to properly represent the dynamics. Finally, assumption (iii) on the ready availability of control resources is not generally an issue in simulations. However, in the laboratory, control resources are always limited, and the key issue is to establish their adequacy in any particular application.

While this work focused on scalar, time-dependent controls $c(t)$, the landscape analysis may be generalized to include controls taken from other elements of the Hamiltonian; specifically, through considerations from quantum system engineering, the analysis can be extended to include control of the Hamiltonian structure itself [27]. In addition, to fully explore the control landscape, trajectories on intermediate level sets [i.e., at a fixed value of $P_{i\to f}(T)$ within the $[0,1]$ window] may be taken by moving along a path locally orthogonal to the landscape gradient [31]. The results of the level-set exploration at the top of the landscape in Sec. VI indicate that the structure of optimal fields can vary significantly; thus, an important direction for future study is NLS control mechanism analysis. The Dyson expansion in Sec. IV proved to be useful to aid in understanding mechanisms tied to examination of the spectral structure of the control field and the Hessian eigenvectors. In addition, an extension of the Hamiltonian encoding technique [43] to the NLS should be valuable for detailed mechanism analysis, especially in complex cases with strong controls and nonlinearities.

In summary, the quantum control landscape analysis for the NLS opens up a wide variety of directions of future work, including examination of new objectives, resources, systems, and mechanism. While the complexity of nonlinear quantum dynamics leaves open many questions, the results of this work offer a promising outlook for future experimental control of the NLS.

ACKNOWLEDGMENT

The authors acknowledge support from the NSF (Grant No. CHE-0718610) and DOE (Grant No. DE-FG02-02ER15344).

[1] I. Carusotto and C. Ciuti, Rev. Mod. Phys. **85**, 299 (2013).
[2] F. Dalfovo, S. Giorgini, L. Pitaevskii, and S. Stringari, Rev. Mod. Phys. **71**, 463 (1999).
[3] S. N. Fisher, A. J. Hale, A. M. Guénault, and G. R. Pickett, Phys. Rev. Lett. **86**, 244 (2001).
[4] N. G. Berloff and B. V. Svistunov, Phys. Rev. A **66**, 013603 (2002).
[5] N. G. Parker and C. S. Adams, Phys. Rev. Lett. **95**, 145301 (2005).
[6] M. Kobayashi and M. Tsubota, Phys. Rev. A **76**, 045603 (2007).
[7] C. N. Weiler, T. W. Neely, D. R. Scherer, A. S. Bradley, M. J. Davis, and B. P. Anderson, Nature (London) **455**, 948 (2008).
[8] E. A. L. Henn, J. A. Seman, G. Roati, K. M. F. Magalhães, and V. S. Bagnato, Phys. Rev. Lett. **103**, 045301 (2009).
[9] K. S. Johnson, J. H. Thywissen, N. H. Dekker, K. K. Berggren, A. P. Chu, R. Younkin, and M. Prentiss, Science **280**, 1583 (1998).
[10] A. S. Bell, B. Brezger, U. Drodofsky, S. Nowak, T. Pfau, J. Stuhler, Th. Schulze, and J. Mlynek, Surf. Sci. **433**, 40 (1999).
[11] O. Zobay, E. V. Goldstein, and P. Meystre, Phys. Rev. A **60**, 3999 (1999).
[12] R. Sewell *et al.*, J. Phys. B: At., Mol. Opt. Phys. **43**, 051003 (2010).
[13] A. K. Tuchman and M. A. Kasevich, Phys. Rev. Lett. **103**, 130403 (2009).
[14] A. Günther, M. Kemmler, S. Kraft, C. J. Vale, C. Zimmermann, and J. Fortágh, Phys. Rev. A **71**, 063619 (2005).
[15] T. Byrnes, K. Wen, and Y. Yamamoto, Phys. Rev. A **85**, 040306(R) (2012).
[16] G. K. Brennen, C. M. Caves, P. S. Jessen, and I. H. Deutsch, Phys. Rev. Lett. **82**, 1060 (1999).
[17] A. Borzì and U. Hohenester, SIAM J. Sci. Comput. **30**, 441 (2008).
[18] U. Hohenester, P. K. Rekdal, A. Borzì, and J. Schmiedmayer, Phys. Rev. A **75**, 023602 (2007).
[19] J. Grond, G. von Winckel, J. Schmiedmayer, and U. Hohenester, Phys. Rev. A **80**, 053625 (2009).
[20] S. Pötting, M. Cramer, and P. Meystre, Phys. Rev. A **64**, 063613 (2001).
[21] S. L. Cornish, N. R. Claussen, J. L. Roberts, E. A. Cornell, and C. E. Wieman, Phys. Rev. Lett. **85**, 1795 (2000).
[22] Z. P. Karkuszewski, K. Sacha, and J. Zakrzewski, Phys. Rev. A **63**, 061601(R) (2001).

[23] P. G. Kevrekidis, G. Theocharis, D. J. Frantzeskakis, and B. A. Malomed, Phys. Rev. Lett. **90**, 230401 (2003).
[24] C. Chin, R. Grimm, P. Julienne, and E. Tiesinga, Rev. Mod. Phys. **82**, 1225 (2010).
[25] H. Rabitz, M. Hsieh, and C. Rosenthal, Science **303**, 1998 (2004).
[26] H. Rabitz, T.-S. Ho, M. Hsieh, R. Kosut, and M. Demiralp, Phys. Rev. A **74**, 012721 (2006).
[27] V. Beltrani, J. Dominy, T.-S. Ho, and H. Rabitz, J. Chem. Phys. **134**, 194106 (2011).
[28] C. Joe-Wong, T.-S. Ho, R. Long, H. Rabitz, and R. Wu, J. Chem. Phys. **138**, 124114 (2013).
[29] R.-B. Wu, A. Pechen, H. Rabitz, M. Hsieh, and B. Tsou, J. Math. Phys. **49**, 022108 (2008).
[30] A. Rothman, T.-S. Ho, and H. Rabitz, Phys. Rev. A **72**, 023416 (2005).
[31] A. Rothman, T.-S. Ho, and H. Rabitz, Phys. Rev. A **73**, 053401 (2006).
[32] S. Weinberg, Ann. Phys. (NY) **194**, 336 (1989).
[33] S. Weinberg, Phys. Rev. Lett. **62**, 485 (1989).
[34] C. M. Dion and E. Cancès, Phys. Rev. E **67**, 046706 (2003).
[35] G. L. Alfimov, P. G. Kevrekidis, V. V. Konotop, and M. Salerno, Phys. Rev. E **66**, 046608 (2002).
[36] Y.-S. Wang and C.-S. Chien, J. Comput. Appl. Math. **235**, 2740 (2011).
[37] T. Kapitula and P. Kevrekidis, Nonlinearity **18**, 2491 (2005).
[38] E. Kirr, P. Kevrekidis, E. Shilzerman, and M. Weinstein, SIAM J. Math. Anal. **40**, 566 (2008).
[39] C. Wang, G. Theocharis, P. G. Kevrekidis, N. Whitaker, K. J. H. Law, D. J. Frantzeskakis, and B. A. Malomed, Phys. Rev. E **80**, 046611 (2009).
[40] V. Ramakrishna, M. V. Salapaka, M. Dahleh, H. Rabitz, and A. Peirce, Phys. Rev. A **51**, 960 (1995).
[41] H. Fu, S. Schirmer, and A. Solomon, J. Phys. A: Math. Gen. **34**, 1679 (2001).
[42] S. Schirmer, I. Pullen, and A. Solomon, J. Phys. A: Math. Gen. **35**, 2327 (2002).
[43] A. Mitra and H. Rabitz, Phys. Rev. A **67**, 033407 (2003).
[44] J.-T. Hwang, E. Dougherty, S. Rabitz, and H. Rabitz, J. Chem. Phys. **69**, 5180 (1978).
[45] A. L. Gaunt, T. F. Schmidutz, I. Gotlibovych, R. P. Smith, and Z. Hadzibabic, Phys. Rev. Lett. **110**, 200406 (2013).